

# Residual stresses of diamond and diamondlike carbon films

Cite as: J. Appl. Phys. **98**, 073515 (2005); <https://doi.org/10.1063/1.2071451>

Submitted: 11 January 2005 . Accepted: 24 August 2005 . Published Online: 10 October 2005

E. Liu, L. Li, B. Blanpain, and J. P. Celis



View Online



Export Citation

## ARTICLES YOU MAY BE INTERESTED IN

[Effect of residual stress on the Raman-spectrum analysis of tetrahedral amorphous carbon films](#)

Applied Physics Letters **78**, 631 (2001); <https://doi.org/10.1063/1.1343840>

[Thermal stability and relaxation in diamond-like-carbon. A Raman study of films with different  \$sp^3\$  fractions \(ta-C to a-C\)](#)

Applied Physics Letters **74**, 2936 (1999); <https://doi.org/10.1063/1.123971>

[Raman spectroscopy on amorphous carbon films](#)

Journal of Applied Physics **80**, 440 (1996); <https://doi.org/10.1063/1.362745>

Applied Physics Reviews  
Now accepting original research

2017 Journal  
Impact Factor:  
**12.894**

# Residual stresses of diamond and diamondlike carbon films

E. Liu<sup>a)</sup> and L. Li*School of Mechanical and Aerospace Engineering, Nanyang Technological University, 50 Nanyang Avenue, Singapore 639798, Singapore*

B. Blanpain and J. P. Celis

*Department of Metallurgy and Materials Engineering, Catholic University of Leuven, de Croylaan 2, B-3001 Leuven, Belgium*

(Received 11 January 2005; accepted 24 August 2005; published online 10 October 2005)

This paper evaluated the internal stresses of different diamond and diamondlike carbon (DLC) coatings. For the diamond coatings, the stresses were determined using micro-Raman spectroscopy and x-ray diffraction (XRD), while the stresses of DLC films were determined with bent plate method. The internal stress was related to the structural properties of the coatings. Direct current plasma jet, combustion flame, and microwave chemical-vapor deposition processes were used to prepare the diamond coatings on the tungsten carbide or molybdenum substrates, while the DLC films were deposited on the silicon wafers with filtered cathodic vacuum arc process. From the Raman spectra of the diamond coatings, the compressive internal stresses were determined, which were related to the microstructure of the coatings. The results from XRD were comparable with those obtained from micro-Raman spectroscopy. Higher compressive residual stresses in the DLC films were noticed, which were also related to their chemical bonding nature as well as their microstructures. © 2005 American Institute of Physics. [DOI: 10.1063/1.2071451]

## I. INTRODUCTION

Residual stress is one of the key aspects for diamond and diamondlike carbon (DLC) coatings as it influences the stability of films on substrates. The internal stress is normally composed of intrinsic stress and thermal stress.<sup>1</sup> The intrinsic stress is generally caused by the interfacial mismatch and structural difference between film and substrate, while the thermal stress is induced by the difference of thermal-expansion coefficients between film and substrate materials during deposition. For the production of diamond and DLC coatings with vapor deposition processes, it is believed that substrate temperature and bias, gas type and flow rate, and substrate material are predominant parameters in determining the structure, morphological characteristics, and residual stress level of the coatings.<sup>2-6</sup>

It was reported that direct current plasma jet (DCPJ) diamond coatings had an internal stress gradient along the radial direction of sample surface.<sup>7</sup> The internal stress of microwave chemical-vapor-deposited (MWCVD) diamond coatings was also investigated.<sup>8</sup>

For DLC coatings deposited at low temperatures, the thermal stress is not important. Their bonding structure, defect density, and amorphous structure determine their stress level. It was reported that an extremely high stress was present in DLC films deposited via filtered cathodic vacuum arc (FCVA),<sup>9</sup> while the internal stresses of some other types of DLC films were not so high,<sup>10</sup> such as a type of boron-doped DLC:B films.<sup>11</sup>

The residual stress of diamond coatings can be determined with x-ray diffraction (XRD),<sup>12,13</sup> Raman

scattering,<sup>3,14-16</sup> or bent plate method.<sup>17</sup> The XRD can be used to obtain an integral stress value in a relatively large area while micro-Raman spectroscopy can acquire stress information in a local area.

For the DLC films, the bent plate method<sup>17</sup> is still a convenient method to evaluate the stress of these films, although it was suggested that Raman spectroscopy be also used to identify the internal stress of DLC films.<sup>18</sup>

This paper evaluates the internal stresses of different diamond and DLC coatings. The morphology and structure are related to the internal stress of these materials.

## II. EXPERIMENTAL DETAILS

Three types of diamond coatings, namely, combustion flame (CF), MWCVD, and DCPJ coatings, and DLC films with or without nitrogen doping produced with FCVA were investigated. A (100) diamond (IIa) and a diamond powder sample were involved as purity and stress-free references.

Table I summarizes the deposition parameters of the coatings. The details of the preparation conditions for the samples used in this study have been described elsewhere.<sup>7,19,20</sup>

Scanning electron microscopy (SEM) (Philips 515), optical microscopy, surface profilometry (Taylor-Hobson and Tencor P10), and atomic force microscopy (AFM) (Digital Instruments, S3000) were used to measure the microstructure of the samples.

The sample surface roughness such as Ra and Rt was evaluated using the surface profilometer operated with a pyramidal diamond stylus scanning the sample surface with a cutoff of 0.25–4 mm depending on the sample surface finishing.

<sup>a)</sup>Author to whom correspondence should be addressed; FAX: +65-67911859; electronic mail: mejliu@ntu.edu.sg

TABLE I. Deposition conditions of diamond and DLC coatings.

Parameter	DCPJ <sup>a</sup>	MW <sup>b</sup>	CF <sup>b</sup>	DLC <sup>c</sup>
Ar	3500 L/h	...	...	...
H <sub>2</sub>	100–500 L/h	250 SCCM	...	...
CH <sub>4</sub>	0.2 L/min	7 SCCM	...	...
H <sub>2</sub>	20 L/min	...	...	...
O <sub>2</sub>	0–0.8 L/min	...	1.5 L/min	...
C <sub>2</sub> H <sub>2</sub>	...	...	1.58 L/min	...
Power	4.2–14 kW	4–5 kW	...	~1.5 kW
Subs. material	Mo	WC–Co	WC–Co	Si wafer
Subs. temp.	900 °C	800–1050 °C	850±20 °C	22 °C
Pressure	60–200 mbars	1–1.25 × 10 <sup>4</sup> Pa	...	~4 × 10 <sup>-7</sup> Torr
Distance (target/subs.)	2.5–4 cm	...	0.7 mm	1 m
Duration	1 h	3–6 h	~1 h	1.5–5 min

<sup>a</sup>Reference 7.<sup>b</sup>Reference 19.<sup>c</sup>Reference 20.

Micro-Raman spectroscopy with a 514.5 nm Ar-ion laser of 15–50 mW was used to obtain the structural information of the diamond samples and further to evaluate their internal stresses. The laser beam was focused on the sample surface with an optical microscope with a magnification of 100× (laser spot size ~2 μm). The Raman spectra were acquired in a range between 1280 and 1380 cm<sup>-1</sup> to evaluate the internal stress.

Two types of XRD measurements, namely, phase and residual stress analyses, on the diamond coatings and reference diamond powder were performed using a Siemens D500 goniometer with Cu Kα radiation (50 kV and 40 mA) in a continuous mode at a low incident-beam angle (0.6°–2°) in order to reduce the influence from the substrates. The detector was equipped with a grazing incidence attachment with Soller slits and LiF monochromator. The slit width and height were fixed at 0.5 and 5 mm, respectively. The XRD patterns were acquired at 2θ from 40° to 145° for phase identification. The integration time and step (2θ) for each data point were 2 s and 0.04°, respectively. For the stress measurement, the acquisition time and step (2θ) for each data point were 7 s and 0.02°, respectively.

For the stress measurement of the DLC samples, the Stoney equation was employed.<sup>17</sup> The surface radii of curvature of Si wafers were measured using surface profilometer before and after the film deposition.

The thicknesses of the diamond coatings were measured with SEM from the fractured cross sections of the coatings. First, a deep notch on the backside of the sample was made by a spark erosion machine, and then the sample was broken by hands. For the DLC films, the thickness was measured with phase-modulated spectral ellipsometer (Jobin Yvon UVISSEL).

### III. RESULTS AND DISCUSSION

For the internal stress measurement with Raman spectroscopy for the behavior of a triply degenerate phonon in a cubic crystal under a hydrostatic strain, the hydrostatic (spherical) component of strain  $\bar{\epsilon}$  for a hydrostatic stress state is expressed as

$$\bar{\epsilon} = (\epsilon_x + \epsilon_y + \epsilon_z)/3. \quad (1)$$

The shift of the Raman phonon line under the hydrostatic stress  $\Delta\omega_H$  is then given by

$$\Delta\omega_H = -3\omega_0\gamma\bar{\epsilon} \text{ (cm}^{-1}\text{)}, \quad (2)$$

where  $\gamma$  is the mode Grüneisen parameter<sup>21</sup> and  $\omega_0$  is the frequency of the particular phonon in question.

Grimsditch *et al.*<sup>22</sup> obtained a mode Grüneisen parameter of 1.06±0.08 or 1.12 from the least-squares fit using the expressions given in (Refs. 23 and 24) for the positions of the singlets and doublets as a function of applied stress. For the  $k \sim 0$  optical mode of diamond, Drickamer *et al.*<sup>25</sup> obtained a mode Grüneisen parameter of 0.94±0.10 using elastic constant data. For the state of plane stress in a diamond coating with principal stresses in two directions parallel to the coating surface being equal, supposing that the diamond coating is an isotropic elastic solid, namely,

$$\sigma_x = \sigma_y, \quad (3)$$

$$\sigma_z = 0, \quad (4)$$

$$\epsilon_x = \epsilon_y = [\sigma_x - \nu(\sigma_z + \sigma_y)]/E = \sigma_x(1 - \nu)/E, \quad (5)$$

$$\epsilon_z = [\sigma_z - \nu(\sigma_x + \sigma_y)]/E = -2\sigma_x\nu/E, \quad (6)$$

from Eq. (1), we have

$$\bar{\epsilon} = (\epsilon_x + \epsilon_y + \epsilon_z)/3 = (1 - 2\nu)(\sigma_x + \sigma_y + \sigma_z)/3E. \quad (7)$$

Since the bulk modulus of elasticity  $K$  has the relation

$$K = E/3(1 - 2\nu), \quad (8)$$

Eq. (2) becomes

$$\begin{aligned} \Delta\omega_H &= -3\omega_0\gamma\bar{\epsilon} = -3\omega_0\gamma(1 - 2\nu)(\sigma_x + \sigma_y + \sigma_z)/3E \\ &= -2\omega_0\gamma\sigma_x/3K \text{ (cm}^{-1}\text{)}. \end{aligned} \quad (9)$$

For bulk diamond,  $E=1141$  GPa,  $K=442$  GPa,  $\nu=0.07$ ,  $\omega_0=1332.5$  cm<sup>-1</sup>, and  $\gamma=0.94$  (Ref. 25) or  $\gamma=1.12$ ,<sup>22</sup> it follows

$$\Delta\omega_H = -1.89\sigma_x \text{ or } \Delta\omega_H = -2.25\sigma_x. \quad (10)$$

TABLE II. Surface morphological characteristics of the samples.

Sample	Ra ( $\mu\text{m}$ )	Rt ( $\mu\text{m}$ )	Thickness ( $\mu\text{m}$ )	Grain size ( $\mu\text{m}$ )
DCPJ1	7.43 $\pm$ 0.9	73.54 $\pm$ 16.34	30–110	10–90
DCPJ2	4.21–5.33	31.44–61.94	...	6–40
MW1	0.57 $\pm$ 0.15	5.88 $\pm$ 1.47	6.8	1–7
MW2	0.43 $\pm$ 0.06	4.31 $\pm$ 1.01	3.9	1–4
MW3	0.26 $\pm$ 0.05	3.03 $\pm$ 0.52	5.5	1–5
CF	0.32 $\pm$ 0.02	4.62 $\pm$ 0.80	10.1	3–8
DLC	0.023 $\pm$ 0.003	0.19 $\pm$ 0.09	0.025–0.066	...

When the Grüneisen parameter of 1.12 is used to calculate the internal stresses of diamond materials, we have

$$\sigma_x = -\Delta\omega_H/2.25 \text{ (GPa)}. \quad (11)$$

In the XRD measurement, the accurate position of a diffraction angle  $2\theta_{(hkl)}$  can be determined from the respective XRD spectrum and further the lattice spacing  $d_{(hkl)}$  is calculated correspondingly. The relative deviation of the lattice spacing in the diamond coatings from that of the stress-free diamond powder sample  $d_{0(hkl)}$  is related to the balanced biaxial stress,  $\sigma_x$  or  $\sigma_y$  ( $\sigma_x = \sigma_y$ ),

$$\begin{aligned} \frac{d_{(hkl)} - d_{0(hkl)}}{d_{0(hkl)}} &= \sigma_x [2s_1 + (s_2/2)] \left[ 1 - \frac{s_2/2}{2s_1 + (s_2/2)} \cos^2 \psi \right] \\ &= \varepsilon_\psi, \end{aligned} \quad (12)$$

where  $\psi$  is the angle between the bisector of incident and diffracted beams and the normal to the sample surface in an  $\omega$  goniometer,  $s_1$  and  $s_2$  are the elastic constants, and  $\varepsilon_\psi$  is the strain corresponding to the selected diffraction plane ( $hkl$ ) caused by the balanced biaxial stresses. At a low incident beam angle  $\alpha$  the angle  $\psi$  is dependent on the  $\alpha$  and selected diffraction plane,

$$\psi = \theta - \alpha. \quad (13)$$

The  $s_1$  and  $s_2$  fundamentally depend on the plane indices. When using mechanical elastic constants, it follows

$$\frac{d_{(hkl)} - d_{0(hkl)}}{d_{0(hkl)}} = \varepsilon_x \left( 1 - \frac{1+\nu}{1-\nu} \cos^2 \psi \right) = \varepsilon_\psi, \quad (14)$$

where  $\varepsilon_x = \varepsilon_y = (1-\nu)\sigma_x/E$  is under the assumption that the coatings are treated as a homogeneous elastic medium.

The detailed surface morphology of the stationary DCPJ sample (DCPJ1) has been demonstrated elsewhere,<sup>7</sup> where large-size and well-faceted diamond crystallites with a (111) preferred orientation were noticed in the central region of diamond-coated area, and then the crystal size reduced towards the outer region of the diamond-coated area. For the translated DCPJ diamond coating (DCPJ2), the trend of surface morphological and structural changes along the transverse direction of strip-shaped diamond coated area is similar to the sample DCPJ1. The surface roughness, crystal size, and coating thickness are summarized in Table II.

The thickness of the DCPJ1 diamond coating from SEM ranges from 30 to 110  $\mu\text{m}$ . A larger thickness in the central region can be observed in Fig. 1.

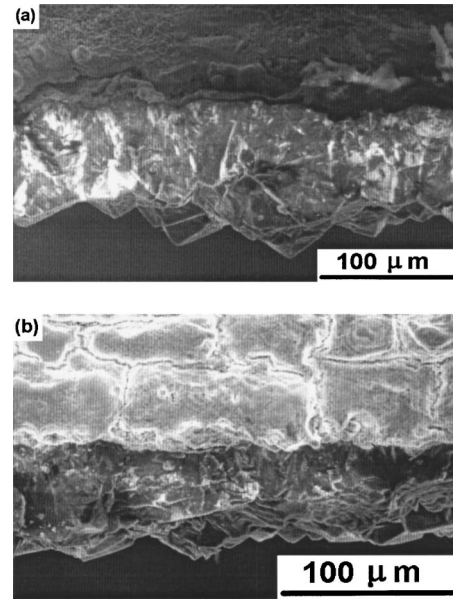


FIG. 1. SEM micrographs of the cross sections of DCPJ1 diamond-coated area: (a) center and (b) near outer region.

The Raman analysis<sup>7</sup> has revealed that the central region of diamond-coated area of DCPJ1 has a higher purity. Then  $sp^2$  contamination gradually develops towards the outer region of the diamond-coated area. The diamond-related peaks across the diamond-coated area are in the range between 1335.3 and 1337.6  $\text{cm}^{-1}$ , while the corresponding Raman peak for the reference bulk diamond is at 1332.5  $\text{cm}^{-1}$  (Fig. 2). A positive Raman shift deviation indicates that a compressive internal stress is present in a diamond coating. The internal stresses are calculated with Eq. (11) and summarized in Table III. The stress distribution across the diamond-coated area is likely related to the thickness distribution and the inhomogeneity in the structure and morphology of the DCPJ diamond coatings. However, more evident  $sp^2$  contamination was noticed even in the central region of DCPJ2. The translation movement of plasma jet on the sample during deposition may have caused such contamination.

The clear diamond peaks can be seen from the XRD spectra of the DCPJ samples (Fig. 3). No major difference between the DCPJ1 and DCPJ2 samples is noticed from the XRD spectra.

The microwave (MW) diamond coatings show well-defined crystal facets (Fig. 4). A mixture of (111) and (110)

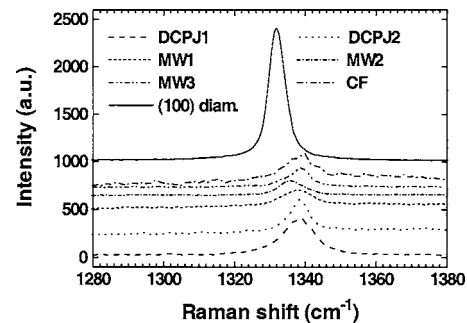


FIG. 2. Raman spectra of different diamond coatings. (100) bulk diamond is used as a reference.

TABLE III. Internal stresses measured on the diamond coatings with micro-Raman spectroscopy and XRD.

Sample	Raman peak (cm <sup>-1</sup> )	Peak FWHM (cm <sup>-1</sup> )	Peak deviation (cm <sup>-1</sup> )	Stress from Raman (GPa)	Stress from XRD (GPa)	<i>sp</i> <sup>2</sup> / <i>sp</i> <sup>3</sup>
Ref. diamond	1332.5	4.5	0	0	0	0
MW1	1337.4±0.1	10.4±0.9	4.9±0.1	-2.18±0.04	-2.47±0.04	7.43 (0.315) <sup>a</sup>
MW2	1335.7±0.1	8.7±0.6	3.2±0.1	-1.42±0.04	-1.98±0.16	1.43 (0.082)
MW3	1337.4±0.1	7.0±0.6	4.9±0.1	-2.18±0.04	-2.39±0.07	2.97 (0.146)
DCPJ1 (Central region)	1337.6±0.5	10.5±1.2	5.1±0.5	-2.27±0.22	-2.02±0.25	0.325 (0.045)
DCPJ2 (Central region)	1338.1±0.4	6.2±0.9	5.6±0.4	-2.49±0.17	-2.45±0.14	13.90 (0.463)
CF	1338.4±0.2	9.3±0.6	5.9±0.2	-2.62±0.1	-2.38±0.07	24.2 (1.358)

<sup>a</sup>The values of *sp*<sup>2</sup>/*sp*<sup>3</sup> in parentheses were derived from the ratios of the amplitudes of *sp*<sup>2</sup> *G* band to those of *sp*<sup>3</sup> diamond peak.

orientations is identified for samples MW1 and MW2 while the component (110) looks predominant. Sample MW3 depicts a predominant (111) crystal orientation as shown in Fig. 4. The thicknesses of the MW diamond coatings are about 6.8 μm for MW1, 3.8 μm for MW2, and 5.5 μm for MW3. The average grain size of MW1 is the largest. The roughness values show dependence on the diamond crystal size and surface finishing (Table II). From the Raman spectra (Fig. 2), clear diamond peaks around 1335–1337 cm<sup>-1</sup> can be observed. The XRD spectra illustrate well-defined diamond peaks (Fig. 3).

From Table III, the compressive internal stresses of the MW diamond coatings obtained from both Raman spectroscopy and XRD are almost at the same level, except sample MW2 for which a relatively evident difference between two kinds of measurements can be noticed. The reason may be that the coating surface of MW2 is not well-densified sideways.<sup>19</sup> It should be noted that the laser beam diameter amplified by the optical microscope in the micro-Raman spectroscopy is about 2 μm, while the XRD results are integral values from a considerably larger measuring area. The laser beam can be focused on a single diamond grain, while the x-ray beam can cover a large number of diamond crystallites. For MW1 and MW3, the matching results from the XRD and Raman measurements are possibly due to their denser microstructures. The thickness and crystal size of the coatings may also be responsible for the stress level.

As demonstrated in Ref. 19, the CF diamond coatings have significant *sp*<sup>2</sup> carbon contamination. However, a clear diamond Raman peak around 1338.2 cm<sup>-1</sup> is identified (Fig. 2). From the XRD spectrum, the diamond characteristic can also be resolved (Fig. 3). The CF diamond coatings show the

highest compressive internal stress level among the diamond-coated samples as indicated in Table III. The *sp*<sup>2</sup>-bonded carbon trapped in the *sp*<sup>3</sup>-bonded diamond crystallites or in the grain boundaries causes more lattice strains in the diamond coating, although a continuous diamond film is still observed in Fig. 5.

The reciprocal difference of the radii of curvature of Si wafers before and after DLC film deposition is used to determine the residual stresses of DLC films  $\sigma_f$  with the formula

$$\sigma_f = \frac{E_s t_s^2}{6(1 - \nu_s) t_f} \left( \frac{1}{R_c} - \frac{1}{R_s} \right), \quad (15)$$

where  $E_s = 180$  GPa,  $\nu_s = 0.26$ ,  $R_s$ , and  $t_s$  are Young's modulus, Poisson's ratio, radius of curvature, and thickness of Si wafer, respectively,  $R_c$  is the composite radius of curvature of film coated substrate, and  $t_f$  is the thickness of DLC film.

The DLC films showed broad and weak Raman bands as reported in Ref. 26. A high content of *sp*<sup>3</sup> carbon bonding in the DLC films is believed to be responsible for the weak feature of the Raman peaks, because the Raman phonon line is more sensitive to the *sp*<sup>2</sup> carbon bonding.

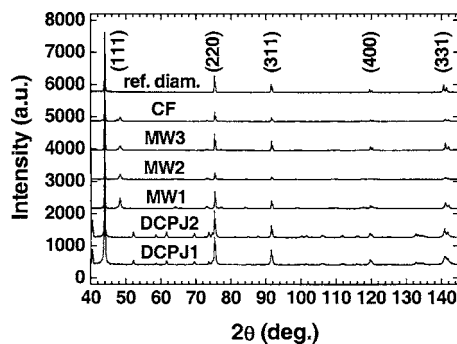


FIG. 3. XRD analysis on different diamond coatings. Diamond powder sample is used as a reference.

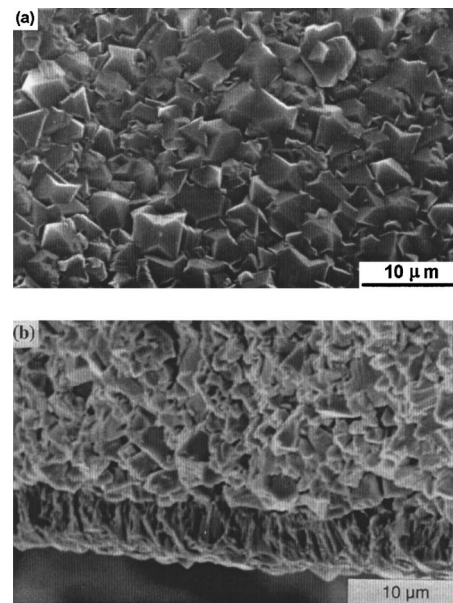


FIG. 4. SEM micrographs of sample MW3: (a) surface morphology and (b) cross section.

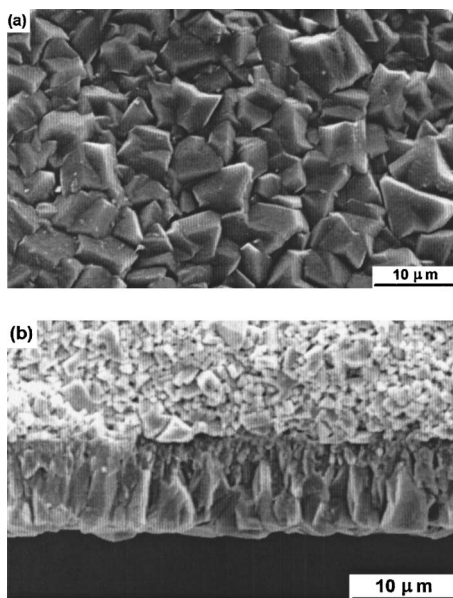


FIG. 5. SEM micrographs of CF diamond coating: (a) surface morphology and (b) cross section.

By calculation with Eq. (15), the internal stresses derived for the DLC films are 8–10 GPa, while that of the nitrogenated DLC films range from 4 to 8 GPa. The influence of nitrogen doping on the internal stress appears to be not very significant. The internal stress up to 10 GPa is too high for the mechanical compliance of the DLC materials. It was reported<sup>27</sup> that a synthetic diamond had a compressive strength of about 6 GPa. Supposing that DLC materials have compressive strengths similar to that of the synthetic diamond, it can be expected that the DLC films may peel off the substrates if their compressive stresses are comparable with their compressive strengths. In reality, the compressive strengths of DLC materials should be lower than that of diamond even when they contain a high content of  $sp^3$  carbon bonding. Therefore, a high compressive stress likely causes the DLC films to be unstable.

Nitrogen atoms can form single bonds, double bonds, and even triple bonds with carbon atoms, which may partially lower the stress during deposition. However, if excessive nitrogen is involved in the film, more  $sp^2$  double bonds in the film are anticipated. In this case, a possible decrease of internal stress in the film is at the expense of its mechanical and optical properties. Since the pure carbon DLC and nitrogen-doped DLC films were deposited at room temperatures, the thermal stress in the films can reasonably be ignored. Therefore, only the intrinsic stresses exist in the films, which are caused by the structural characteristics of these amorphous materials.

#### IV. CONCLUSIONS

The internal stresses of diamond and DLC coatings were evaluated with respect to their microstructural characteristics.

The variation of Raman peak shift of diamond coatings relative to the reference diamond was noticed, from which the compressive internal stresses were derived.

The DCPJ diamond coatings contained a stress gradient along the radial direction of the coating surfaces, while the internal stresses in the MW and CF samples were more uniform.

A higher internal stress in the CF diamond coatings compared to that of the DCPJ and MW diamond coatings was due to more  $sp^2$ -bonded carbon contamination in the CF coatings.

The DLC films illustrated much higher internal stresses compared to the diamond coatings, which was related to their amorphous nature and chemical bonding structure.

<sup>1</sup>F. M. d'Heurle, *Thin Solid Films* **171**, 81 (1989).

<sup>2</sup>S. K. Choi, D. Y. Jung, and H. M. Choi, *J. Vac. Sci. Technol. A* **14**, 165 (1996).

<sup>3</sup>J. A. N. Goncalves, G. M. Sardonato, and K. Iha, *Diamond Relat. Mater.* **11**, 1578 (2002).

<sup>4</sup>S. Miyagawa, S. Nakao, M. Ikeyama, and Y. Miyagawa, *Surf. Coat. Technol.* **156**, 322 (2002).

<sup>5</sup>Q. H. Fan, A. Fernandes, E. Pereira, and J. Gracio, *J. Appl. Phys.* **84**, 3155 (1998).

<sup>6</sup>J. Jeong, D. Kwon, W. S. Lee, and Y. J. Baik, *J. Appl. Phys.* **90**, 1227 (2001).

<sup>7</sup>E. Liu, B. Blanpain, J. P. Celis, J. R. Roos, G. A. Vervens, and Th. Priem, *Surf. Coat. Technol.* **80**, 264 (1996).

<sup>8</sup>P. K. Bachmann, H. D. Bausen, H. Lade, D. Leers, and D. U. Wiechert, *Diamond Relat. Mater.* **3**, 1308 (1994).

<sup>9</sup>E. Liu, X. Shi, B. K. Tay, L. K. Cheah, H. S. Tan, J. R. Shi, and Z. Sun, *J. Appl. Phys.* **86**, 6078 (1999).

<sup>10</sup>A. Grill, V. Patel, and B. Meyerson, *Surf. Coat. Technol.* **49**, 530 (1991).

<sup>11</sup>M. Chhowalla, Y. Yin, G. A. J. Amaratunga, D. R. McKenzie, and Th. Frauenheim, *Appl. Phys. Lett.* **69**, 2344 (1996).

<sup>12</sup>H. Guo and M. Alam, in *Applications of Diamond and Related Materials*, edited by Y. Tzeng, M. Yoshikawa, M. Murakawa, and A. Feldman (Elsevier, Amsterdam, 1991), pp. 149.

<sup>13</sup>N. S. VanDamme, D. C. Nagle, and S. R. Winzer, *Appl. Phys. Lett.* **58**, 2919 (1991).

<sup>14</sup>E. Gheeraert, A. Deneuille, A. M. Bonnot, and L. Abello, *Diamond Relat. Mater.* **1**, 525 (1992).

<sup>15</sup>C. Johnston, A. Crossley, P. R. Chalker, I. M. Buckley-Golder, and K. Kobashi, *Diamond Relat. Mater.* **1**, 450 (1992).

<sup>16</sup>M. Yoshikawa, G. Katagiri, H. Ishida, A. Ishitani, M. Ono, and K. Matsumura, *Appl. Phys. Lett.* **55**, 2608 (1989).

<sup>17</sup>G. G. Stoney, *Proc. R. Soc. London, Ser. A* **82**, 172 (1909).

<sup>18</sup>J. W. Ager III, S. Anders, A. Anders, and L. G. Brown, *Appl. Phys. Lett.* **66**, 3444 (1995).

<sup>19</sup>E. Liu, B. Blanpain, and J. P. Celis, *Diamond Relat. Mater.* **5**, 649 (1996).

<sup>20</sup>X. Shi, M. Fulton, D. Flynn, B. K. Tay, and H. S. Tan, *Deposition Apparatus*, PCT/GB96/00390, 20 February 1995.

<sup>21</sup>S. S. Mitra, O. Brafman, W. B. Daniels, and R. K. Crawford, *Phys. Rev.* **186**, 942 (1969).

<sup>22</sup>M. H. Grimsditch, E. Anastassakis, and M. Cardona, *Phys. Rev. B* **18**, 901 (1978).

<sup>23</sup>F. Cerdeira, C. J. Buchenauer, F. H. Pollak, and M. Cardona, *Phys. Rev. B* **5**, 580 (1972).

<sup>24</sup>S. Venugopalan and A. K. Ramdas, *Phys. Rev. B* **8**, 717 (1973).

<sup>25</sup>H. G. Drickamer, R. W. Lynch, R. L. Clendenen, and E. A. Perez-Albuerne, *Solid State Phys.* **19**, 135 (1966).

<sup>26</sup>E. Liu, B. Blanpain, X. Shi, J.-P. Celis, H.-S. Tan, B.-K. Tay, L.-K. Cheah, and J. R. Roos, *Surf. Coat. Technol.* **106**, 72 (1998).

<sup>27</sup>P. D. Ownby and R. R. W. Stewart, in *Engineering Materials Handbook*, edited by S. J. Schneider (ASM International, Handbook Committee, U.S.A., 1991), Vol. 4, p. 821.